Microphase Separation vs Crystallization in Polystyrene-*b*-polybutadiene-*b*-poly(ϵ-caprolactone) ABC Triblock Copolymers

V. Balsamo,*,† C. Urbina de Navarro,‡ and G. Gil‡

Grupo de Polímeros USB, Departamento de Ciencia de los Materiales, Universidad Simón Bolívar, Aptdo. 89000, Baruta 1080A, Caracas, Venezuela, and Centro de Microscopía Electrónica, Facultad de Ciencias, Universidad Central de Venezuela, Caracas, Venezuela

Received January 25, 2002

ABSTRACT: The melting behavior as well as the crystallization kinetics of a series of polystyrene-*b*-polybutadiene-*b*-poly(ϵ-caprolactone) ABC triblock copolymers was investigated by differential scanning calorimetry (DSC). The studies were performed as a function of annealing time at high temperature (150 °C), maintaining invariable the crystallization conditions. While a copolymer with only 16 wt % PCL does not show significant changes with the annealing time, it influences strongly the melting behavior and crystallization kinetics of copolymers with higher PCL content. Thus, higher melting points and degree of crystallinity can be observed by increasing annealing time, suggesting the results show a clear "conflict" between microphase separation and crystallization. This is more evident when the thermodynamic force to form spherulites and the thermodynamic force to maintain the microphase morphology formed in the melt compete. The analysis of the crystallization kinetics through the Avrami theory demonstrated that when the nucleation step proceeds heterogeneously, the Avrami exponent effectively reflects the dimensionality of crystal growth.

Introduction

The crystallization behavior of diblock copolymers has been extensively investigated during several years in polyethylene (PE),[1−5] poly(ϵ-caprolactone) (PCL),[6−10] or poly(ethylene oxide) (PEO)[8,11−13] containing systems.[14−17] This kind of materials provide well-defined model systems for studying self-assembly because the composition and interactions can be controlled over a wide range. It has been found from these studies that the crystallization process and final morphology relate intimately to the microdomain structure existing in the melt, glass transition of linked amorphous blocks, and level of segregation. On cooling from the melt, structural changes from crystallization compete with those due to microphase separation, and final morphology depends on whether crystallization is confined or unconfined.[3,16,18,19] Crystallization may take place within an existent mesophase templated by the prior microphase separation if it occurs in a strongly segregated block copolymer or in block copolymers containing glassy blocks.[5,20−22] On the other hand, if crystallization occurs in a weakly segregated block copolymer or directly from a disordered phase, it will control the final microphase morphology.[1,2,7,17,23]

Several time-resolved studies have investigated the crystallization of diblock copolymers from both homogeneous and weakly segregated melts.[1,2,4,10,16,24] As expected for semicrystalline materials that form a spherulitic superstructure, the crystallization was well represented by the Avrami equation.[2,7] The presence of an ordered melt mesophase presents, however, an added complexity to the crystallization process. Register et al.[3] reported that when crystallization proceeds from a strongly segregated melt in E/MB diblock copolymers and crystallization is confined in cylinders, the behavior seems not to be reflected in the value of the Avrami parameter *n*. However, when crystallization was confined into spheres in a E/SEB diblock copolymer, it was well described by the Avrami equation.[5] A value of the Avrami parameter $n = 1$ was obtained because the spheres were homogeneously nucleated due to the fact that the number of microdomains far exceeds the possible number on impurities in the sample. Chen et al.[25] also showed that the crystallinity development in cylindrical and spherical morphologies obeys a simple exponential function prescribed by the first-order kinetics. This first-order kinetic behavior along with the exceedingly large undercooling verified the homogeneous nucleation in these two types of mesophases. The idea that homogeneous nucleation could be prevalent in block copolymers with crystallizable minority blocks and a vitreous matrix was put forth originally by Lotz and Kovacs and supported by the work of Robitaille and Prud'homme.[26,27]

Although the situation may seem more or less clear in semicrystalline diblock copolymers, the interplay crystallization−microphase separation is much more complex when semicrystalline ABC triblock copolymers are considered. These systems are very attractive because the unique morphologies that are possible to obtain with them. While the microphase morphology of ABC triblock copolymers has been intensively studied in amorphous systems, the understanding of the phase behavior and crystallization process in semicrystalline ABC systems has yet to be realized. At this respect, the first reports were given by Balsamo et al. [28−30] in polystyrene-*b*-polybutadiene-*b*-poly(ϵ-caprolactone) triblock copolymers and their hydrogenated versions. Copolymers with a minority of the crystallizable block are able to effectively confine crystallization in such a way that fractionated crystallization can take place with

* To whom correspondence should be addressed. E-mail: vbalsamo@usb.ve.
† Universidad Simón Bolívar.
‡ Universidad Central de Venezuela.

10.1021/ma020128w CCC: $25.00
Published on Web 05/23/2003

Table 1. Molecular Characteristics of the Triblock Copolymers Used in the Present Study

copolymer[a]	$M_{n(cop)}$ (kg/mol)[b]	$M_{n(PCL)}$ (kg/mol)	M_w/M_n
$S_{57}B_{27}C_{16}$	137	22	1.12
$S_{51}B_{09}C_{40}$	98	39	1.15
$S_{25}B_{26}C_{49}$	84	41	1.15
$S_{27}B_{15}C_{58}$	219	127	1.30

[a] Subscripts represent the weight percent of each component. [b] Determined from ^{1}H NMR using $M_{n(PS)}$ obtained from GPC curves, calibrated with PS standards.

a combination of heterogeneous and homogeneous nucleation.[29] More recently, it has been demonstrated that such behavior is general for semicrystalline ABC triblock copolymers with one or two confined semicrystalline blocks.[31,32] In addition, the occurrence of morphological transitions has been demonstrated by changing the crystallization conditions.[33] Nevertheless, most studies that investigate the relationship between crystallization and microphase morphology have focused their attention on the morphology dependence with the crystallization conditions (time and temperature), while only a few reports that relate directly the final microphase morphology with the thermal behavior on melting can be found in the literature. Nojima et al.[10] were able to observe morphological transitions by studying the melting process of crystallized PCL-*b*-PB by SR−SAXS and differential scanning calorimetry. They studied the general melting behavior by changing composition and crystallization temperature.

Since the reports have been limited to study morphological changes that can take place during melting or by crystallizing under different crystallization conditions, we investigate in detail the melting behavior as well as the crystallization kinetics of polystyrene-*b*-polybutadiene-*b*-poly(ϵ-caprolactone) triblock copolymers that were subjected to different annealing conditions at high temperature in the melt, maintaining invariable the crystallization conditions. We study the crystallization kinetics by using the Avrami equation to analyze the primary crystallization, while in a forthcoming contribution[34] we explore in detail the correlation between the thermal behavior and microdomain morphology.

Experimental Part

Materials. Table 1 shows the molecular characteristics of the polystyrene-*b*-polybutadiene-*b*-polycaprolactone triblock copolymers used in the present study. These block copolymers were synthesized via sequential living anionic polymerization as was described in an earlier work.[35] The absence of the rest of the homopolymers (PS and PCL) and diblock copolymer (PS-*b*-PCL) was confirmed by GPC experiments as detailed in ref 35.

Polymer films of ∼1 mm thickness were slowly cast from 5% w/v toluene solutions at room temperature. Then, they were introduced into a vacuum oven at room temperature for 3 days to eliminate solvent traces. Samples of the films were taken to follow a thermal treatment (see Table 2) under nitrogen atmosphere.

Differential Scanning Calorimetry (DSC). Samples (15 ± 1 mg) were encapsulated in aluminum pans, and high purity dry helium was used as inert atmosphere in a Perkin-Elmer DSC Pyris 1. The instrument was calibrated with cyclohexane and indium.

Standard "TT0" cooling and heating DSC scans (10 °C/min) between 150 °C and −120 °C were carried out erasing the crystalline history of untreated samples (after solvent casting) by holding them for 3 min at 150 °C. Heating DSC scans (10 °C/min) of "treated" samples (TT2, TT3, and TT4) were performed from −120 up to +150 °C.

Table 2. Thermal Treatments Applied to the Block Copolymers

thermal treatment	time at 150 °C (h)	T_c (°C)	time at T_c (h)[a]
TT2	5	40	5
TT3	10	40	5
TT4	15	40	5

[a] The cooling rate from 150 °C to T_c was approximately 0.5 °C/min. After 5 h at T_c the samples were quenched in liquid nitrogen.

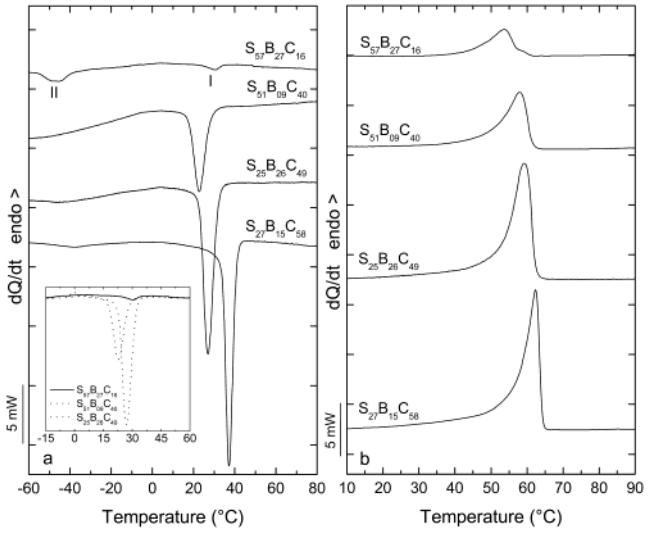

Figure 1. Standard TT0 DSC (a) cooling and (b) heating scans (10 °C/min) of the copolymers used in the present study. The inset shows a magnification and superposition of the different crystallization exotherms.

For continuous isothermal crystallizations, samples TT2 and TT4 ($S_{51}B_{09}C_{40}$, $S_{25}B_{26}C_{49}$, and $S_{27}B_{15}C_{58}$) were taken. The crystalline history of each sample was erased by holding it for 3 min at 150 °C. Then, a fast cooling (60 °C/min) down to a crystallization temperature T_c was performed. At that temperature the sample was held for a time t_c, which we selected to be four times the time to reach the crystallization minimum at that T_c. Finally, the sample was heated at 10 °C/min up to 150 °C. This procedure was repeated at least for six temperatures for each copolymer with thermal treatment TT2 and for $T_c = 40$ °C for each copolymer with thermal treatment TT4. It should be mentioned that a new sample was taken for each isothermal crystallization in order to avoid possible morphological changes by repeatedly heating of the samples up to 150 °C.

Because of the low PCL content in $S_{57}B_{27}C_{16}$ the isothermal crystallization of this copolymer was done after erasing the thermal history using the procedure "by step" described as follows:

(a) Fast cooling (60 °C/min) from 150 °C down to T_c.

(b) Sample held at T_c for a time t_c, which was increased in the subsequent steps.

(c) Heating at 10 °C/min from T_c to 150 °C.

(d) Three minutes at 150 °C.

Steps a−d were repeated at the same T_c, but at increasing t_c. The last t_c was taken as the time that the melting enthalpy in the subsequent heating scan did not change with respect to the previous one.

Results and Discussion

Prior to the discussion of the influence of sample preparation conditions on thermal properties, we present in Figure 1 the "standard TT0" thermal behavior of the block copolymers under study. This figure shows the exotherms and endotherms corresponding to the

Table 3. Thermal Transitions Obtained from "standard TT0" DSC Scans

sample	$T_{c(I)}$ (°C)	$T_{c(II)}$ (°C)	% X_C	$T_{m(I)}$ (°C)	$T_{m(II)}$ (°C)	% X_m
$S_{57}B_{27}C_{16}$	30.5	−45.3	27	53.6	58.2	45
$S_{51}B_{09}C_{40}$	22.7		35	58.0		41
$S_{25}B_{26}C_{49}$	27.1		51	58.7		61
$S_{27}B_{15}C_{58}$	37.2		47	59.5		56

Table 4. Glass Transitions Obtained from "standard TT0" DSC Heating Scans

sample	$T_{g(PB)}$ (°C)	$T_{g(PCL)}$ (°C)	$T_{g(PS)}$ (°C)
$S_{57}B_{27}C_{16}$	−99.0	*a*	94.0
$S_{51}B_{09}C_{40}$	−92.0	−67.1	92.7
$S_{25}B_{26}C_{49}$	−96.6	−62.2	94.9
$S_{27}B_{15}C_{58}$	−93.0	−62.2	82.0

[a] Because of the low PCL content it could not be detected.

crystallization and melting of the PCL block, which is the crystallizable component in these materials. For $S_{51}B_{09}C_{40}$, $S_{25}B_{25}C_{49}$, and $S_{27}B_{15}C_{58}$, only one crystallization exotherm is observed in Figure 1a. This exotherm $T_{c(I)}$ is shifted from 22.7 °C in $S_{51}B_{09}C_{40}$ to higher temperatures (see Table 3) as the PCL content increases. $S_{57}B_{27}C_{16}$ exhibits, in addition, a second wide exotherm, exotherm II, at high undercoolings (−45.3 °C). Such behavior has been previously attributed to a fractionated crystallization phenomenon [29,31] that is promoted by the presence of a number of isolated microdomains (10^{15}/cm^3),[34] which is higher than the number of heterogeneities usually present in a PCL homopolymer (10^7/cm^3).[31] Therefore, exotherm I is caused by heterogeneous nucleation and exotherm II probably by homogeneous nucleation, due to its closeness to the PCL glass transition. This fractionated crystallization explains the apparently higher crystallization temperature, $T_{c(I)}$ of $S_{57}B_{27}C_{16}$ compared to $S_{51}B_{09}C_{40}$ and $S_{25}B_{26}C_{49}$ (see Table 3). As can be observed in the inset of Figure 1a, exotherm I of $S_{57}B_{27}C_{16}$ is located comparatively in the high temperature tail of the exotherms of the other copolymers. This indicates, considering that only ∼20% of the PCL present in $S_{57}B_{27}C_{16}$ crystallizes in exotherm I, that what we are looking in peak I is a small crystal fraction that is being nucleated by the most active heterogeneities present in the sample. In fact, the analysis of the subsequent heating curves in Figure 1b shows that there is no increase of the melting temperature of $S_{57}B_{27}C_{16}$ with respect to the other copolymers, corroborating that the apparently higher $T_{c(I)}$ is due to a nucleation effect and not to the formation of thicker crystals.

In the subsequent heating (see Figure 1b) a shift of the melting peak to lower temperatures is observed as the PCL content decreases. It is interesting to note that the crystallinity degree obtained from heating scans is considerably higher than those calculated from cooling scans. This indicates that annealing of the crystals is taking place during heating, especially in the copolymer with only 16% PCL, in which an increase in the crystallinity from 27% to 45% takes place during heating. This represents an increase of about 67% with respect to the initial value. The reason for this marked increase is that the crystallization in this copolymer of a material fraction (0.8) at very high undercooling leads to the formation of metastable crystals, which change during heating to give more perfect crystals.

Table 4 shows the glass transition of each component obtained for the standard samples. The presence of the PCL, PB, and PS glass transitions evidences that these copolymers are microphase separated at least until temperatures as high as 90 °C. In $S_{25}B_{26}C_{49}$ the PS glass transition could not be unambiguously determined from the standard heating scan, probably due to the low PS content and some overlapping with the PCL melting endotherm. Then, the following experiment was done. The sample was heated to 150 °C, held for 3 min at that temperature, cooled to 50 °C, and heated immediately up to 150 °C. This experiment avoided the presence of the PCL melting endotherm and allowed an unambiguous determination of $T_{g(PS)}$.

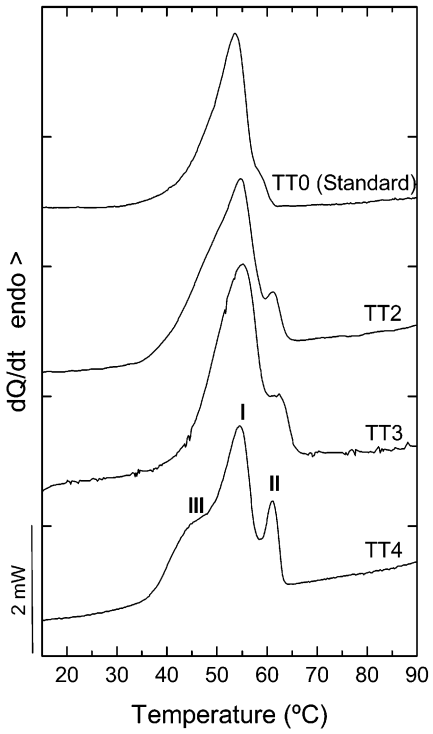

Figure 2. DSC heating scans (10 °C/min) after thermal treatments for $S_{57}B_{27}C_{16}$.

As mentioned in the experimental part, the treated samples were annealed at 150 °C for different times (5, 10, and 15 h), and on the basis of the "standard" crystallization behavior, 40 °C was selected as the crystallization temperature for the thermal treatments. It should be emphasized that to our knowledge all previous works reported in semicrystalline block copolymers have been limited to study the thermal behavior by changing crystallization conditions. In this work, the main objective was to study the thermal behavior by changing the annealing conditions at high temperature.

Figure 2 presents the heating DSC scans obtained for $S_{57}B_{27}C_{16}$ after the samples were prepared by solvent casting, annealed at 150 °C and crystallized at T_c for 5 h. It is interesting to observe that a change in the annealing time at 150 °C (without varying crystallization conditions) produces a complex melting behavior of the PCL block with a multimodal endotherm that is better defined at longer annealing times. To discard that the multimodal distribution of lamellar thicknesses could be due to degradation of the polymer, some GPC experiments were performed. No changes were observed. However, it is known that sometimes small changes cannot be properly detected in the GPC curves, whereas the thermal behavior can reflect them. Then,

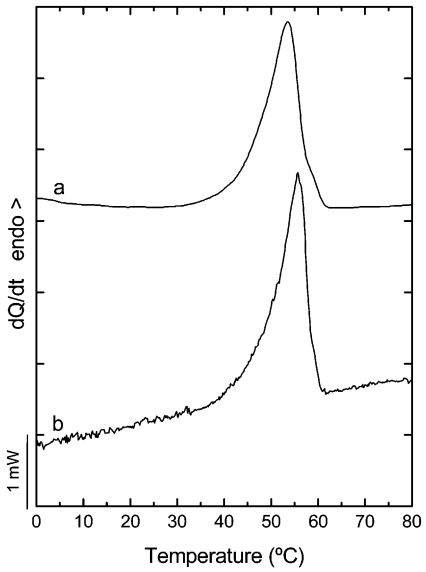

Figure 3. DSC heating scans (10 °C/min) of $S_{57}B_{27}C_{16}$: (a) standard TT0; (b) sample TT4 after a controlled cooling at 10 °C/min from +150 down to −120 °C.

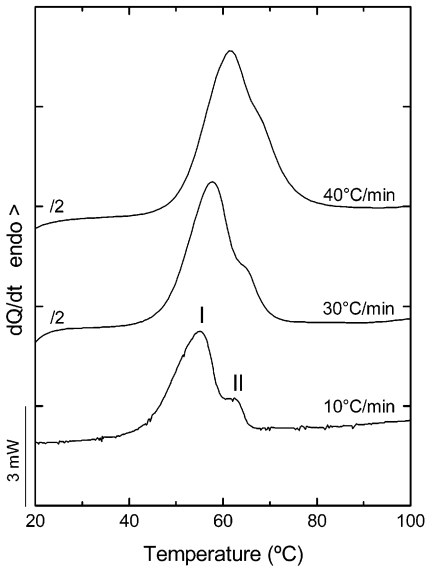

Figure 4. DSC heating scans of $S_{57}B_{27}C_{16}$ TT3 performed at different heating rates.

a treated sample TT4 was heated to 150 °C for 3 min, cooled at 10 °C/min, and reheated. As can be appreciated in Figure 3 the multimodal melting disappears and an increase of the melting temperature in TT4 is observed with respect to TT0. This, indicates that the multimodal endotherms of Figure 2 were caused by the isothermal crystallization within the morphology generated after the annealing at 150 °C and not due to a degradation of the material. In addition, it should be mentioned that the slight increase of the melting temperature of curve b in Figure 3 with respect to the standard scan occurs, since, once the morphology has been "equilibrated" at 150 °C, it is not destroyed by a heating to 150 °C.[34]

Multiple endotherms arise usually from recrystallization during DSC measurements, i.e., imperfect crystals melt and recrystallize into more perfect crystals. In fact, Berghmans et al.[12] and Booth et al.[17] reported such effect in PEO-*b*-PCL and PEO-*b*-POB block copolymers, respectively. To elucidate the nature of the multimodal melting endotherms, samples TT3 were heated at different heating rates (see Figure 4). The two melting peaks widen when the heating rate increases from 10 to 40 °C/min, but they do not merge into one peak. Moreover, a measurement of the relative height (Δh) of the melting endotherms showed that, in contrast to what would be expected if some partial melting−recrystallization was taken place, $\Delta h_{(I)}/\Delta h_{(II)}$ exhibited an increase from 2.84 to 3.78 by lowering the heating rate from 40 to 10 °C/min. Therefore, the occurrence of multiple melting does not result from recrystallization when heating in the course of the DSC heating scan. Thus, the phenomenon reflects the complicated crystallization mechanism of the block copolymer. Similar results where obtained by Zhang et al.[8] in PCL-*b*-PEO-*b*-PCL triblock copolymers. The effect can neither be the result of the melting within two different morphologies as reported by Nojima et al.[20] due to the confined nature of the PCL block in $S_{57}B_{27}C_{16}$.[29,34] Then, the multimodal endotherm is due to the formation of different lamellar thicknesses that are consequence of the fractionated crystallization within a morphology that has been equilibrated. Thus, peak II corresponds to the melting of the small fraction of crystals that was nucleated at high temperature and peaks I and III to the crystals

Table 5. Thermal Transitions Obtained for $S_{57}B_{27}C_{16}$ and $S_{27}B_{15}C_{58}$

$S_{57}B_{27}C_{16}$	$T_{m(I)}$ (°C)	$T_{m(II)}$ (°C)	% X_m	$S_{27}B_{15}C_{58}$	$T_{m(I)}$ (°C)	$T_{m(II)}$ (°C)	% X_m
TT0	53.6		45	TT0	59.5		45
TT2	54.7	61.1	54	TT2	61.4	35.1	63
TT3	55.2	61.9	62	TT3	62.2	40.5	66
TT4[a]	55.7	61.1	59	TT4	63.7	43.5	65

[a] A third melting endotherm $T_{m(III)}$ was observed at 43.9°C.

that were nucleated at low temperature. In fact, an analysis of Figure 1a shows that exotherm II seems to be composed by two crystalline populations. The reason for the better definition of the peaks is only observed after the isothermal crystallization is that this process favors a better segregation of the population that melts at high temperature. Simultaneously, annealing at 150 °C also contributes to a better definition of the different lamellar thicknesses I and III.

The values of the melting temperatures and crystallinity degrees corresponding to Figure 2 are presented in Table 5. In $S_{57}B_{27}C_{16}$, the melting temperatures of the annealed samples do not change significantly with the annealing time. Endotherm I in the treated samples is slightly shifted to higher temperatures in comparison to the standard sample, as is expected from an isothermal crystallization. A slight increase of the degree of crystallinity is also observed from TT2 to TT4, indicating that the annealing process, and probably the long-range order reached at higher annealing times,[34] allows the formation of better defined crystalline populations with more PCL crystals. On one hand, this could seem contradictory since a higher ordering of the nanostructures leads to a higher confinement of the semicrystalline block. In fact, there are reports where the confinement of a semicrystalline block in AB diblock copolymers dramatically perturbs the crystallization process.[36] Nevertheless, it should be considered on the other hand, that crystallization in microphase separated morphology with good long-range order could result in higher crystallinity due to lesser amount of grain boundary defects.

To investigate the effect of the thermal treatment on the copolymers by changing composition, we performed

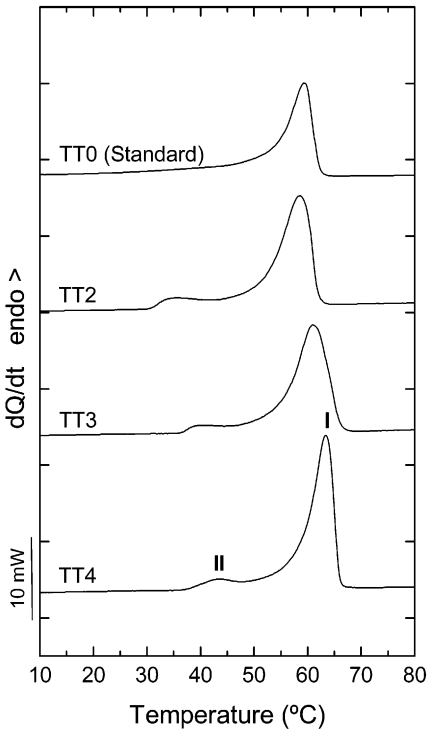

Figure 5. DSC heating scans (10 °C/min) after thermal treatments for $S_{27}B_{15}C_{58}$.

the same analysis for $S_{27}B_{15}C_{58}$. Figure 5 and Table 5 present the corresponding results. Although in this case a multimodal distribution of lamellar thicknesses was not clearly obtained, the effect of the annealing time is much more marked than in $S_{57}B_{27}C_{16}$. Two crystalline populations appear (I and II), which exhibit a significant shift of the melting point to higher values when the annealing time increases, despite the similar crystallization conditions. Simultaneously, as expected, an increase of the degree of crystallinity with respect to the standard sample is observed. Because of its low temperature, peak II cannot be attributed to a secondary crystallization process (in $S_{27}B_{15}C_{58}$ TT2 $T_{m(II)} < T_c$). Peak II is therefore caused by the crystallization of material during the cooling from T_c down to liquid nitrogen temperature.

A comparison of the variation of the melting points for $S_{57}B_{27}C_{16}$ and $S_{27}B_{15}C_{58}$ shows that, despite the similar crystallization conditions, the latter copolymer undergoes a significant lamellar thickening by increasing annealing time. $S_{57}B_{27}C_{16}$, on the other hand, does not show such increase. This indicates as is demonstrated elsewhere for these triblock copolymers[34] that a confining of the semicrystalline component to cylinders in $S_{57}B_{27}C_{16}$ in contrast to confining in lamellae in $S_{27}B_{15}C_{58}$ leads to better stabilization of the morphology during annealing in the first case; i.e., there is not a "conflict" between crystallization and microphase separation. Then, the final morphology is controlled by microphase separation despite the 27% rubbery component. An explanation of this effect requires a detailed knowledge of the morphology under the different conditions, what is presented in a forthcoming publication.[34] Nevertheless, it can be put forward that $S_{27}B_{15}C_{58}$ has a lamellar−lamellar morphology and it can form spherulites under specific conditions.[28,33,34] Under polarized light in the optical microscopy, ~3 μm sections of sample TT2 demonstrated the presence of spherulites, but ~3 μm sections of sample TT4 did not show them. Then,

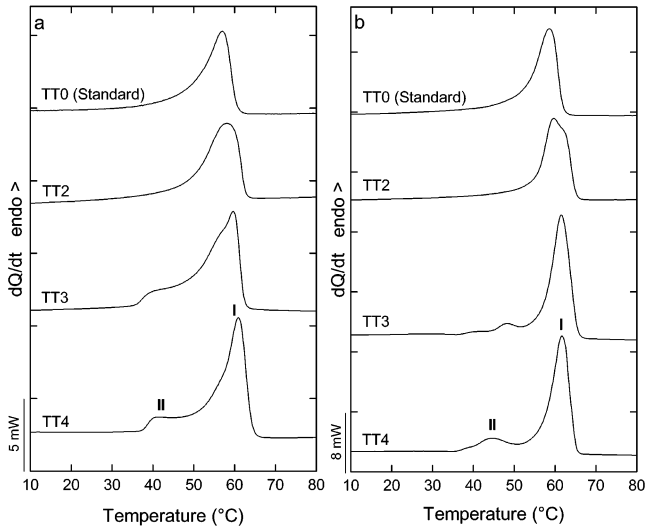

Figure 6. DSC heating scans (10 °C/min) after thermal treatments for (a) $S_{51}B_{09}C_{40}$ and (b) $S_{25}B_{26}C_{49}$.

Table 6. Thermal Transitions Obtained for $S_{51}B_{09}C_{40}$ and $S_{25}B_{26}C_{49}$

$S_{51}B_{09}C_{40}$	$T_{m(I)}$ (°C)	$T_{m(II)}$ (°C)	% X_m	$S_{25}B_{26}C_{49}$	$T_{m(I)}$ (°C)	$T_{m(II)}$ (°C)	% X_m
TT0	58.0		41	TT0	58.7		61
TT2	58.2		54	TT2	60.5		62
TT3	59.8	39.1	59	TT3	61.5	47.9	65
TT4	61.0	40.5	59	TT4	61.5	43.9	65

there is a clear "conflict" between the thermodynamic force to form spherulitic superstructures and the thermodynamic force to maintain the microphase separated morphology formed in the melt. In the sample, TT2 seems to dominate the first one and in the sample, TT4 seems to dominate the second one. The thermal behavior indicates that lamellar thickening is less restricted in sample TT4 where a higher long-range order is reached [34] with the consequence that the melting points that can be reached are higher. Nevertheless, it should be reminded that such lamellar thickening is controlled by the compromise between the random-coil configuration preferred by the amorphous blocks and the extended chain conformation of the crystallites.

Copolymers with 40% and 49% PCL were also analyzed. The thermal behavior of $S_{51}B_{09}C_{40}$ and $S_{25}B_{26}C_{49}$ is presented in Figure 6 and summarized in Table 6. In general, these copolymers exhibit a similar behavior compared to $S_{27}B_{15}C_{58}$; i.e., higher melting points are obtained with increasing annealing time. The change is not so marked like in $S_{27}B_{15}C_{58}$ and the melting points are between those of $S_{57}B_{27}C_{16}$ and $S_{27}B_{15}C_{58}$ revealing an intermediate situation due to the PCL content. However, samples TT2 in $S_{51}B_{09}C_{40}$ and $S_{25}B_{26}C_{49}$ did not exhibit the second endotherm, indicating that microphase morphology and, therefore, the long-range order reached in the melt allows or inhibits the formation of a defined crystal population with low melting point, probably located at the interfaces. Despite the unambiguous determination of the glass transitions in $S_{25}B_{26}C_{49}$ TT2, this sample did not exhibit an ordered morphology in the electronic microscope.[34] It should be highlighted that like in $S_{57}B_{27}C_{16}$, these copolymers were not able to build spherulites, being then absent the strong "conflict" between spherulite formation and microphase separation, reason for what the variation of the melting points with increasing annealing time is less pronounced than in $S_{27}B_{15}C_{58}$.

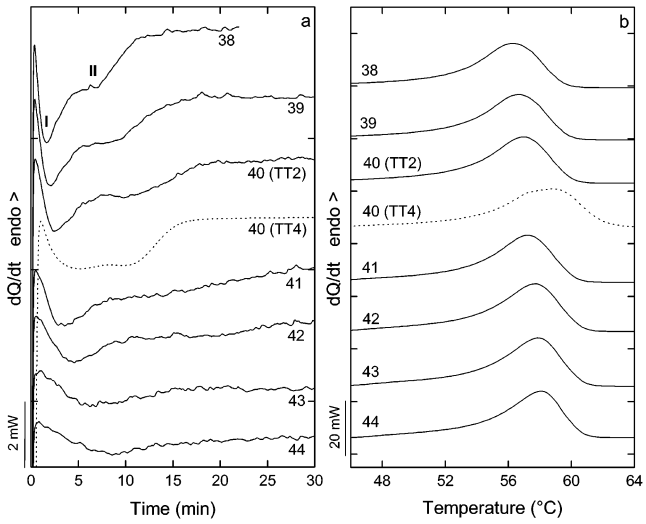

Figure 7. Isothermal DSC curves and subsequent heating scans (10 °C/min) for $S_{25}B_{26}C_{49}$ TT2. The dotted lines correspond to the isothermal crystallization at T_c = 40 °C and subsequent heating scan of $S_{25}B_{26}C_{49}$ TT4.

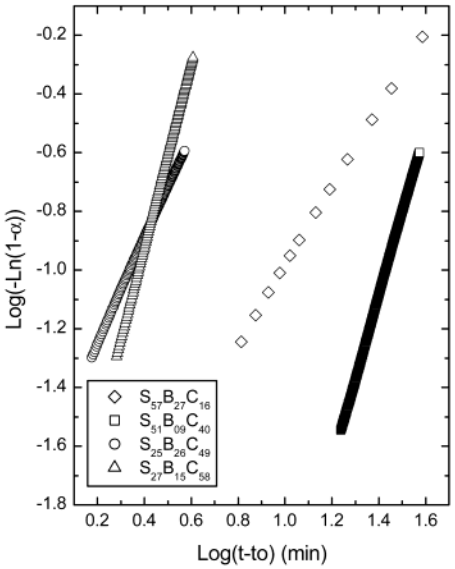

Figure 8. Avrami plots for PCL crystallization at T_c = 40 °C within samples TT4.

The crystallization kinetics was also studied in this work through isothermal crystallizations that were performed in the differential scanning calorimeter for samples $S_{27}B_{15}C_{58}$, $S_{25}B_{26}C_{49}$, and $S_{51}B_{09}C_{40}$ TT2 at different temperatures and TT4 at 40 °C. For $S_{57}B_{27}C_{16}$ TT2 and TT4, the procedure applied for crystallization was the step isothermal crystallization described in the experimental part, and it was performed only at T_c = 40 °C in both cases. Figure 7 illustrates the isothermal curves and subsequent heating scans for $S_{25}B_{26}C_{49}$, which exhibited an unusual behavior during crystallization. Sample TT2 exhibits a main crystallization exotherm I with a higher time shoulder (II) at low crystallization temperatures. Nevertheless, such bimodality is not observed in the subsequent heating scan. In our opinion two explanations are possible. The first one could be an overlapping of the melting of two crystalline populations during the heating scan; in fact, it can be observed that the melting endotherm is relatively broad. On the other hand, the two exotherms could correspond to crystallization in two different morphologies that coexist at such crystallization temperature due to metastability in the morphology. In fact, this sample did not exhibit an ordered morphology in the electron microscope.[34] Therefore, we performed the isothermal crystallization of sample $S_{25}B_{26}C_{49}$ TT4 at 40 °C, which exhibits a lamellar−lamellar morphology. The result is plotted in Figure 7a with a dotted line. Although the bimodality does not disappear, the ratio of the minima changes, indicating that a morphological transition is taking place in agreement with TEM observations.[34]

From the isothermal crystallizations we were able to carry out the study of the crystallization kinetics according to Avrami theory:[37]

$$\alpha(t) = 1 - \exp[-k(t - t_o)^n] \qquad (1)$$

where $\alpha(t)$ is defined as the volumetric fraction of material that crystallized at time t, n, and k are the Avrami exponent and the overall crystallization rate constant respectively, and t_o represents the induction period for crystallization. The application of this equation must be very careful, since there are many factors that can affect the results.[38] It is usual to find conflicting results for the Avrami parameters in the literature, even when homopolymers are being evaluated.[39] These conflicting results can be attributed to the way in which the calculations are performed. Some of the errors, when DSC is used, are normally due to the estimation of t_o and ΔH_c. The degree of conversion to the crystalline state until which the linear fit is carried out is very important. For these reasons we were very strict in the estimation of the different experimental parameters. This is reflected in linear correlation factors higher than 0,999 for all experiments. We applied eq 1 to several conversion ranges, to be sure that we were not taken a range where secondary crystallization occurs.

Figure 8 shows as example Avrami plots for samples TT4. As mentioned above, very good linear relationships can be observed, a fact that makes possible the calculation of n and k during primary crystallization. The results for all copolymers are reported in Table 7. Previous works[17,25,40,41] have reported that confinement of a semicrystalline block within a segregated diblock copolymer can radically alter polymer crystallization in such way that crystallization within spherical or cylindrical mesophases leads to a crystallization that follows a first-order kinetics due to the occurrence of homogeneous nucleation. On the other hand, crystallization within interconnected structures such as the gyroid follows a more conventional sigmoidal kinetics.[41] Nevertheless, the extent of interconnectivity can generate intermediate situations with a combination of homogeneous and heterogeneous nucleation that affect the crystallization kinetics. The richness of morphologies that is possible to obtain within semicrystalline triblock copolymers lead us, then, to study the crystallization kinetics in our materials. $S_{51}B_{09}C_{40}$ and $S_{25}B_{26}C_{49}$ show in Table 7 Avrami exponents that vary between 1.7 and 2.9. Taking into account that samples TT2 of $S_{51}B_{09}C_{40}$ and TT4 of $S_{25}B_{26}C_{49}$ exhibit lamellar−cylindrical and lamellar−lamellar morphologies,[34] a crystallization that proceeds from homogeneous nucleation would be expected with a resulting first-order kinetics. Nevertheless, values higher than 1 were obtained. This suggests that the PCL lamellae should be connected across the grain boundaries or defects such

Table 7. Avrami Parameters Obtained for Different Crystallization Temperatures

copolymer	TT	T_c (°C)	n	log k (seg^{-n})	$t^{1/2}$ (min)
$S_{57}B_{27}C_{16}$	2	40	1.38	−2.13	26.8
	4	40	1.34	−2.32	39.8
$S_{51}B_{09}C_{40}$	2	28	1.54	−0.98	2.9
		29	1.73	−1.45	3.6
		30	1.83	−1.73	4.4
		31	1.82	−1.89	4.9
		32	1.86	−2.27	6.5
		34	1.86	−2.52	9.5
		40	1.98	−3.64	55.2
	4	40	2.86	−5.10	55.0
$S_{25}B_{26}C_{49}$	2	37	1.71	−0.79	3.2
		38	1.74	−1.01	3.9
		39	1.79	−1.21	5.2
		40	1.73	−1.54	6.2
		41	1.88	−1.68	9.5
		42	1.90	−1.92	11.2
		43	1.94	−2.09	13.9
		44	2.02	−2.31	13.9
	4	40	1.78	−1.60	6.9
$S_{27}B_{15}C_{58}$	2	34	3.28	0.29	1.0
		35	3.35	−0.06	1.2
		36	3.58	−0.61	1.7
		37	3.68	−0.97	2.1
		38	3.78	−1.39	2.5
		39	3.83	−1.88	3.2
		40	4.05	−2.33	3.4
		41	3.93	−2.29	5.4
		42	4.17	−3.64	7.4
	4	40	3.15	−2.18	4.4

as screw dislocations.[41−43] It is noteworthy the fact that for $S_{51}B_{09}C_{40}$ the Avrami exponent changes at 40 °C from 2.0 in TT2 to 2.9 in TT4, which is in agreement with the morphological findings for this copolymer.[34] Sample TT2 exhibited a lamellar−cylindrical morphology, whereas sample TT4 showed a PCL matrix.

$S_{27}B_{15}C_{58}$ has an Avrami exponent that changes from 4.1 in TT2 to 3.2 in TT4 at 40 °C. This indicates a three-dimensional growth of the superstructures in the first case in agreement with the observation of spherulites through polarized optical microscopy.[28,33] On the other hand, sample TT4 did not exhibit spherulite formation. Then, a value of 3 suggests a bidimensional growth with a nucleation mechanism that is mainly sporadic at the crystallization temperature of 40 °C.

For $S_{57}B_{27}C_{16}$, which forms PCL cylinders, the Avrami exponent was 1.3 and 1.4 for samples TT2 and TT4, respectively. Taking into account that these values correspond to the higher-temperature process of crystallization, it can be concluded from this result and the values obtained for the previous copolymers, that when crystallization proceeds from heterogeneous nucleation the Avrami exponent effectively reflects the dimensionality of crystal growth. A different situation emerges when crystallization proceeds from homogeneous nucleation.[44] In this latter case, Register et al.[41] reported a first-order kinetics whenever crystallization occurs within isolated microdomains, regardless of the microdomain dimensionality.

Figure 9 shows plots of the crystallization half-time data as a function of isothermal crystallization temperature for all samples TT2. The slope of the curves represents the temperature dependence (S) of the overall crystallization rate for each copolymer. Fitting the data of Figure 9 yields $S = 0.100-0.106$/ °C, i.e., the same temperature dependence is obtained for all materials. This demonstrates that when crystallization takes place from heterogeneous nucleation, these materials exhibit similar temperature dependence of the crystallization rate despite the morphological differences between them. Nevertheless, a comparison of the crystallization half-time at a fixed temperature (40 °C) shows that it is composition dependent due to the confinement of the semicrystalline block.

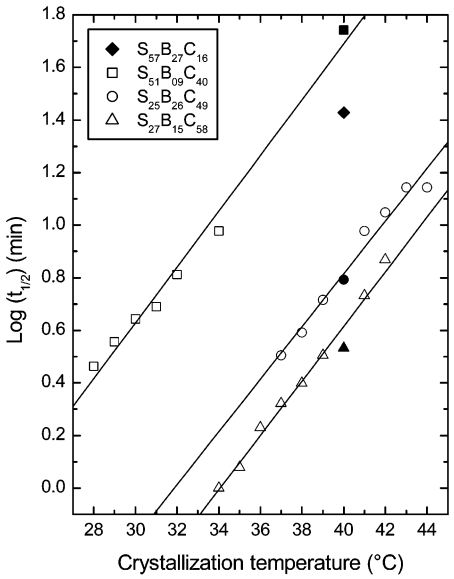

Figure 9. Dependence of crystallization half-time $t_{1/2}$ with crystallization temperature for samples TT4.

Conclusions

The study of the thermal behavior of polystyrene-*b*-polybutadiene-*b*-poly(ϵ-caprolactone) block copolymers with different composition as a function of the annealing time at high temperature, maintaining invariable the crystallization conditions, demonstrated that this is an important parameter that must be considered in the analysis of semicrystalline block copolymers. Although the influence was stronger in triblock copolymers with relatively high PCL contents, it could also be observed that the increase of the annealing time in a copolymer with only 16% PCL led to the definition of different lamellar thicknesses due to an equilibration of the morphology. By increasing the contents of the semicrystalline component, the increase of the annealing time produces higher melting points and higher degree of crystallinity, indicating that confining of the semicrystalline component to lamellae in contrast to confining in cylinders leads to a higher "conflict" between crystallization and microphase separation. Then, when the PCL block is less confined there is clear conflict between the thermodynamic force to form, for example, spherulitic superstructures and the thermodynamic force to maintain the microphase separated morphology formed in the melt. It seems to be that lamellar thickening is less restricted when formation of spherulites does not occur.

From the isothermal crystallizations we were able to carry out the study of the crystallization kinetics according to Avrami theory. The values obtained for the Avrami exponents, higher than one, in copolymers that built PCL−lamellar microdomains, revealed along with the dynamic thermal behavior that the nucleation step is taking place heterogeneously and that the microdomains should be interconnected. It was demonstrated that when crystallization proceeds from heterogeneous nucleation, the Avrami exponent effectively reflects the

dimensionality of crystal growth in contrast to those cases in which nucleation proceeds from homogeneous nucleation.

Acknowledgment. This work was made possible by the financial support of the "Fondo Nacional de Ciencia, Tecnología e Innovación" (FONACIT) through Grant S1-96001934 and of the "Decanato de Investigación y Desarrollo" from Simón Bolívar University through Grant DID-G02. The authors acknowledge Dr. Friederike von Gyldenfeldt for synthesizing some of the copolymers used in the present study. Valuable discussions with A. J. Müller are also acknowledged.

References and Notes

(1) Rangarajan, P.; Register, R. A.; Fetters, L. J.; Naylor, S.; Ryan, A. J. *Macromolecules* **1995**, *28*, 1422.
(2) Ryan, A. J.; Hamley, I. W.; Bras, W.; Bates, F. S. *Macromolecules* **1995**, *28*, 3860.
(3) Quiram, D. J.; Register, R. A.; Marchand, G. R.; Ryan, A. J. *Macromolecules* **1997**, *30*, 8338.
(4) Rangarajan, P.; Register, R. A.; Fetters, L. J.; Bras, W.; Naylor, S.; Ryan, A. J. *Macromolecules* **1995**, *23*, 4932.
(5) Loo, Y. L.; Register, R. A.; Ryan, A. J. *Phys. Rev. Lett.* **2000**, *84*, 18, 4120.
(6) Heuschen, J.; Jerome, R.; Teyssie, P. *J. Polym. Sci., Part B: Polym. Phys.* **1989**, *27*, 523.
(7) Nojima, S.; Nakano, H.; Takahashi, Y.; Ashida, T. *Polymer* **1994**, *35*, 16, 3479.
(8) Gan, Z.; Jiang, B.; Zhang, J. *J. Appl. Polym. Sci.* **1996**, *59*, 961.
(9) Nojima, S.; Fujimoto, M.; Kakihira, H.; Sasaki, S. *Polym. J.* **1998**, *30*, 968.
(10) Nojima, S.; Kikuchi, N.; Rohadi, A.; Tanimoto, S.; Sasaki, S. *Macromolecules* **1999**, *32*, 3727.
(11) Mai, S.; Fairclough, J. P. A.; Viras, K.; Gorry, P. A.; Hamley, I. W.; Ryan, A. J.; Booth, C. *Macromolecules* **1997**, *30*, 8392.
(12) Bogdanov, B.; Vidts, A.; Schacht, E.; Berghmans, H. *Macromolecules* **1999**, *32*, 726.
(13) Nojima, S.; Ono, M.; Ashida, T. *Polym. J.* **1992**, *24*, 11, 1271.
(14) Gervais, M.; Gallot, B.; Jerome, R.; Teyssie, P. *Makromol. Chem.* **1981**, *182*, 989.
(15) Richardson, P. H.; Richards, R. W.; Blundell, D. J.; MacDonald, W. A.; Mills, P. *Polymer* **1995**, *36*, 3059.
(16) Hamley, I. W.; Fairclough, J. P. A.; Bates, F. S.; Ryan, A. J. *Polymer* **1998**, *39*, 1429.
(17) Ryan, A. J.; Fairclough, J. P. A.; Hamley, I. W.; Mai, S. M.; Booth, C. *Macromolecules* **1997**, *30*, 1723.
(18) Hamley, I. W.; Fairclough, J. P. A.; Terrill, N. J.; Ryan, A. J.; Lipic, P. M.; Bates, F. S. *Macromolecules* **1996**, *29*, 8835.
(19) Quiram, D. J.; Register, R. A.; Marchand, G. R. *Macromolecules* **1997**, *30*, 4551.
(20) Hamley, I. W.; Fairclough, J. P. A.; Ryan, A. J.; Bates, F. S.; Towns-Andrews, E. *Polymer* **1996**, *37*, 4425.
(21) Quiram, D. J.; Register, R. A.; Marchand, G. R.; Adamson, D. H. *Macromolecules* **1998**, *31*, 4891.
(22) Zhu, L.; Cheng, S. Z. D.; Calhoun, B. H.; Ge, Q.; Quirk, R. P.; Thomas, E. L.; Hsiao, B. S.; Yeh, F. J.; Lotz, B. *J. Am. Chem. Soc.* **2000**, *122*, 5927.
(23) Rangarajan, P.; Register, R. A.; Fetters, L. J. *Macromolecules* **1993**, *29*, 4640.
(24) Zhu, L.; Calhoun, B. H.; Ge, Q.; Quirk, R. P.; Cheng, S. Z. D.; Thomas, E. L.; Hsiao, B. S.; Yeh, F.; Liu, L.; Lotz, B. *Macromolecules* **2001**, *34*, 1244.
(25) Chen, H. L.; Wu, J. C.; Lin, T. L.; Lin, J. S. *Macromolecules* **2001**, *34*, 6936.
(26) Lotz, B.; Kovacs, A. J. *Polym. Prepr. (Am. Chem. Soc., Div. Polym. Chem.)* **1969**, *10*, 820.
(27) Robitaille, C.; Prud'homme, J. *Macromolecules* **1983**, *16*, 665.
(28) Balsamo, V.; von Gyldenfeldt, F.; Stadler, R. *Macromol. Chem. Phys.* **1996**, *197*, 3317.
(29) Balsamo, V.; von Gyldenfeldt, F.; Stadler, R. *Macromolecules* **1999**, *32*, 1226.
(30) Balsamo, V.; Müller, A. J.; von Gyldenfeldt, F.; Stadler, R. *Macromol. Chem. Phys.* **1998**, *199*, 1063.
(31) Müller, A. J.; Balsamo, V.; Arnal, M. L.; Jakob, T.; Schmalz, H.; Abetz, V. *Macromolecules* **2002**, *35*, 3048.
(32) Arnal, M. L.; Balsamo, V.; López-Carrasquero, F.; Contreras, J.; Carrillo, M.; Schmalz, H.; Abetz, V.; Laredo, E.; Müller, A. J. *Macromolecules* **2001**, *34*, 7973.
(33) Balsamo, V.; Stadler, R. *Macromolecules* **1999**, *32*, 3994.
(34) Balsamo, V.; Gil, G.; Urbina de Navarro, C.; Abetz, V.; von Gyldenfeldt, F.; Hamley, I. W. *Macromolecules*, in press.
(35) Balsamo, V.; von Gyldenfeldt, F.; Stadler, R. *Macromol. Chem. Phys.* **1996**, *197*, 1159.
(36) Nojima, S.; Toei, M.; Hara, S.; Tanimoto, S.; Sasaki, S. *Polymer* **2002**, *43*, 4087.
(37) Mark, J. E.; Ed.; *Physical Properties of Polymers Handbook*; American Institute of Physics: Woodbury, NY, 1996; p 401.
(38) Skoglund, P.; Fransson, A. *J. Appl. Polym. Sci.* **1996**, *61*, 2455.
(39) Balsamo, V.; Calzadilla, N.; Mora, G.; Müller, A. J. *J. Polym. Sci., B: Polym. Phys.* **2001**, *39*, 771.
(40) Chen, H. L.; Wu, J. C.; Lin, T. L.; Lin, J. S. *Macromolecules* **2001**, *34*, 6936.
(41) Loo, Y. L.; Register, R. A.; Ryan, A. J.; Dee, G. T. *Macromolecules* **2001**, *34*, 8968.
(42) Hong, S.; MacKnight, W. J.; Russell, T. P.; Gido, S. P. *Macromolecules* **2001**, *34*, 2876.
(43) Hong, S.; Yang, L.; MacKnight, W. J.; Gido, S. P. *Macromolecules* **2001**, *34*, 7009.
(44) Balsamo, V.; Müller, A. J.; Urdaneta, N.; Carrizales, P.; Gil, G. Manuscript in preparation.

MA020128W